Pure Appl. Chem., Vol. 72, Nos. 1–2, pp. 101–117, 2000.

Synthesis and characterization of Cu_xS nanoparticles. Nature of the infrared band and charge-carrier dynamics*

M. C. Brelle[1], C. L. Torres-Martinez[2], J. C. McNulty[1], R. K. Mehra[2†], and J. Z. Zhang[1†]

[1]Department of Chemistry, University of California, Santa Cruz, California 95064, [2]Department of Neuroscience and Environmental Toxicology Graduate Program, University of California, Riverside, California 92521 USA

Abstract: Cu_xS (x = 1,2) nanoparticles have been synthesized utilizing different capping molecules including polyethyleneglycol (PEG), polyvinylpyrrolidone (PVP), casein hydrolysate-enzymatic (CAS), and bovine serum albumin (BSA). The ground-state electronic absorption spectra of the Cu_xS nanoparticles show three distinct types of Cu_xS formed: a green type assigned as crystalline CuS, and two brown types assigned as crystalline Cu_2S and amorphous Cu_2S. The brown types exhibit a steady increase in absorption toward shorter wavelengths starting at around 650 nm, while the green type shows the same steady increase in absorption, but with an additional absorption band in the infrared (IR). The IR band is attributed to an electron-acceptor state lying within the bandgap. ESR measurements of free Cu(II) ions in solution for all samples show the presence of Cu(II) in the brown amorphous samples, but not in the green or brown crystalline samples. Ultrafast dynamics of photoinduced electrons have been measured for all samples using femtosecond-transient absorption/bleach spectroscopy. In all brown Cu_2S samples studied, the early time-transient profiles feature a pulse-width-limited (<150 fs) rise followed by a fast decay (1.1 ps) and a slow decay (>80 ps). These decay dynamics were found to be independent of pump power and stabilizing agent. The fast 1.1 ps decay is attributed to charge carrier trapping, while the long decay may be due to either recombination or deep trapping of the charge carriers. The green Cu_xS samples studied showed interesting power-dependent behavior. At low excitation intensities, the green Cu_xS samples showed a transient bleach signal, while at high intensities, a transient absorption signal has been observed. The increased transient absorption over bleach at high intensities is attributed to trap-state saturation. A kinetic model has been developed to account for the main features of the electronic relaxation dynamics.

INTRODUCTION

Nanoparticles are of great interest due to their extremely small size and large surface-to-volume ratio, which lead to both chemical and physical differences in their properties compared to bulk of the same chemical composition [1–15]. They offer an excellent opportunity to study the effects of spatial confinement on charge carrier behavior and problems related to surfaces or interfaces. The use of time-resolved techniques allows for direct measurements of charge-carrier dynamics in nanoparticles and helps to better understand effects of size and surface on fundamental properties of charge carriers [15–47].

Pure Appl. Chem.* **72, 1–331 (2000). An issue of reviews and research papers based on lectures presented at the 1st IUPAC Workshop on Advanced Materials (WAM1), Hong Kong, July 1999, on the theme of nanostructured systems.
†Corresponding authors

Metal sulfide nanoparticles have interesting optical and electrical properties, especially with respect to the effect of oxidation on these properties. Aqueous syntheses of metal sulfide nanocrystalline semiconductors can be readily achieved by competing ligand mechanisms. Previous studies have shown that titration of sulfide into stable metallocomplexes of cysteine, glutathione, or phytochelatins results in the controlled synthesis of metal-sulfide nanocrystalline materials [45,48–56]. This work extends the concept of using competing ligand mechanisms for the synthesis of Cu_xS nanoparticles using biomolecules like proteins or synthetic polar materials like polyvinylpyrrolidone as capping agents. Proteins bind soft metals due to the affinity of sulfhydryl or imidazoles groups for Cd^{2+}, Hg^{2+}, and Cu^{2+}. Indeed, the binding and subsequent reduction of Cu^{2+} by cysteines in proteins is the basis for an analytical method for the assay of proteins [57]. It, therefore, seemed logical to try metallocomplexes of proteins as precursors for the synthesis of metal sulfide nanocrystals.

Copper sulfides are a particularly interesting class of metal sulfides due to their ability to form with various stoichiometries. The copper–sulphur system can exist in the chalcocite (Cu_2S) and covellite (CuS) phases with several stable and metastable phases of varying stoichiometry between the two ideal compositions. Their complex structures and valence states result in some unique properties [30,31,58–70]. For example, covellite had been believed to exist in two forms, brown CuS and green CuS, with the latter having an additional absorption band in the IR [60,63,65,66,68,69]. Green CuS has been found to be the true crystalline form of covellite composed of 1/3 Cu(II) and 2/3 Cu(I) [60–62,66,67,70]. Brown CuS has been characterized to be a poor crystalline or amorphous type of covellite, CuS, composed entirely of Cu(I), not Cu(II) [62,66,70]. Since Cu(I)S is apparently not stoichiometrically balanced, the appropriate label should probably be amorphous Cu_2S, as suggested also by others [70]. This is the label we will use in the paper.

It has been observed that the preparation of Cu_xS nanoparticles at 30 °C gives green crystalline CuS (strong IR absorption) with metallic properties, while preparation at 10 °C gives brown amorphous Cu_2S with semiconductor properties [66]. The difference was attributed to the brown sample being in a metastable state, whereas the green sample is the true stable crystalline state of CuS. In a recent study by Drummond et al., CuS nanoparticles were found to have the IR band that disappeared following reduction to Cu_2S via viologen, and was therefore attributed to the presence of Cu(II) [60,70]. The IR band has also been attributed to charge transfer from a CuS core to a Cu–O shell, where the Cu–O shell was formed from oxidation of CuS by way of heating the sample exposed to oxygen [65,68,69]. The nature of this band, as well as its influence on the charge carrier dynamics, is still a matter of discussion.

In this paper we have synthesized Cu_xS nanoparticles with different capping agents, including polymers and biomolecules. We have characterized their optical and dynamic properties using electronic absorption spectroscopy, time-resolved transient absorption and bleach, and electron spin resonance (ESR). The results obtained suggest that the IR band could be due to an electron acceptor state that lies within the bandgap of Cu_xS. The dynamics data indicate that the electronic relaxation is primarily nonradiative and dominated by surface trap states.

EXPERIMENTAL

Synthesis of aqueous Cu_xS stabilized with polyethyleneglycol (PEG)

The Cu_xS nanoparticles were synthesized using two different approaches. The first was to prepare aqueous Cu_xS nanoparticles using a polymer as a capping agent, following a reported procedure [60]. All reagents were purchased from Aldrich. A rapidly stirred solution of milli-Q water containing copper(II) chloride (6.0×10^{-4} M) and 2% polyethyleneglycol (PEG, average mol wt 10 000) cooled in an ice bath was deaerated with argon and then injected with H_2S to form a brown colloid solution of Cu_xS. Half of this

sample was then exposed to air and heated slowly to 70 °C. During heating the solution undergoes a color change from brown to green due to the appearance of an IR absorption band. The brown sample will be hereby-labeled PEG1 and the green sample as PEG2. The nanoparticles have an average size of 10 nm as determined by transmission electron microscopy (TEM). The size did not change noticeably after heating.

Synthesis of Cu_xS capped with polyvinylpyrrolidone (PVP), bovine serum albumin (BSA), and casein hydrolysate-enzymatic (CAS)

The second approach involved a new technique that generated Cu_xS nanoparticles capped with polymer polyvinylpyrrolidone (PVP), or biological molecules including bovine serum albumin (BSA) and casein hydrolysate-enzymatic (CAS). PVP (average mol wt 360 000, molecular biology grade reagent) and BSA (fraction V powder) were purchased from Sigma. Casein was obtained from United States Biochemical Corporation, Cleveland, Ohio. All other routine materials were purchased from Fischer Scientific. Unless specified, all reagents were prepared using degassed and nitrogen-saturated high-quality water (18 MΩ/cm). Capping agents PVP, BSA, and casein were dissolved in distilled water at the indicated concentrations. $CuSO_4$ solutions at desired concentrations were prepared in 0.01N HCl. Sodium sulfide solutions were prepared in degassed water purged with nitrogen. Cu(I) solutions were prepared by the reduction of Cu(II) as follows: (i) 0.5 ml of 0.5 M $CuSO_4$ was reduced with 1.0 ml of 0.5 M ascorbic acid and (ii) 1.0 ml acetonitrile solution was mixed in to obtain a colorless solution. Thus, generated Cu(I) solutions were used immediately. Cu_xS nanoparticles were prepared by competing ligand mechanisms as detailed previously for the synthesis of Ag_2S, CdS and ZnS nanocrystals [45,52–56]. Cu complexes of PVP, BSA, and casein were prepared by titration of Cu(II) or Cu(I) solution into the capping agent. In a typical small-scale synthesis, 2.0 ml of 5% (wt/vol) PVP solution was reacted with 0.05 or 0.1 ml of 0.5 M Cu(II). After a 10-min room temperature incubation, the synthesis of Cu_xS nanoparticles was achieved by titrating in aqueous sodium sulfide to obtain molar sulfide/Cu ratios of 1.0 and 2.0. The samples were thoroughly mixed and purged with nitrogen and stored under nitrogen. The PVP samples will be hereafter labeled as PVP1 (brown) and PVP2 (green). Cu_xS samples capped with BSA were prepared similarly except that BSA concentration was changed to 0.5% (wt/vol) in some experiments. The BSA samples will be here on labeled as BSA1 (brown) and BSA2 (green). However, casein-capped samples were prepared slightly differently. Casein solution (0.5%, wt/vol) was reacted with 0.025 ml of 0.5 M $CuSO_4$. Sodium sulfide was added to obtain sulfide/Cu ratios varying from 0.125 to 1.0. The casein-capped samples were not stable for any extended period of time and were therefore not studied optically. BSA or PVP-capped crystalline Cu_2S samples were prepared similarly with Cu(I) except that Cu(II) solutions were changed to Cu(I) solutions. These samples will be labeled as BSA3, PVP3, and PVP4. Glutathione(GSH) and cysteine were also used in the synthesis of Cu_xS but were not stable for preparation of brown Cu_xS. However, green CuS capped with GSH or cysteine was stable for months at room temperature when kept under nitrogen.

Equipment

ESR spectra were taken for many of the samples to help determine the oxidation state and environment of free Cu ions in solution. ESR measurements were taken with a Bruker ESP-380 FT-EPR with a TE102 cavity at ~110 K. The ground absorption state spectra were taken on a HP-8452A UV-vis spectrometer. TEM measurements were taken on a Jeol-100 CX transmission electron microscope.

The dynamics were performed using a pump-probe scheme with a regeneratively amplified, mode-locked femtosecond Ti-sapphire laser. All samples were prepared to have a ground-state optical density of ~1.0 at 390 nm for laser experiments. The laser system and the experimental set-up have been de-

scribed before [25]. Briefly, pulses of 40 fs duration with 5 μJ/pulse energy at a repetition rate of 100 MHz were generated and amplified in a Ti-sapphire regenerative amplifier using chirped-pulse amplification. The final output pulses obtained were typically 150 fs with pulse energy of 250 μJ, centered at 780 nm at 1 KHz. The amplified output was doubled to generate 20 μJ/pulse of 390-nm light, which was used as a pump source to excite the colloids contained in a quartz cell with a 1-cm optical path length. The remaining fundamental was used to generate a white light continuum, and the desired probe wavelength was selected by using an interference band pass filter. An optical delay line based on a translation stage controlled the delay between pump and probe. The pump and probe beams were focused with a 10-cm focal length lens and cross overlapped over a spot size of 0.5 mm^2 in the sample before the focal point. The pump power was attenuated to such a level (<15 μJ/pulse) that there was no signal observed from the pure solvent, i.e., water, due to multiphoton ionization.

RESULTS

Ground-state electronic absorption

The ground-state absorption spectra of several Cu_xS nanoparticles studied are shown in Fig. 1A–C. The brown amorphous Cu_2S samples shown in Fig. 1A were prepared starting with Cu(II) salts and with different stabilizing agents, PVP1 (solid line), BSA1 (dashed line), or PEG1 (dotted line). The absorption gradually increases toward shorter wavelength starting at ~650 nm and shows no discrete peaks. This steady increase in absorption with decreasing wavelength is typical of indirect bandgap semiconductors. The spectra in Fig. 1B were for the green crystalline CuS samples either by direct preparation or by heating of the brown amorphous Cu_2S sample capped with PVP2 (solid line), BSA2 (dashed line), or PEG2 (dotted line). It can be seen that a new absorption band forms in the IR. Interestingly, during the conversion of the brown sample to the green sample, little absorption change is observed in the visible to UV region while the IR band is being formed. For comparison, the absorption spectra of samples of crystalline Cu_2S prepared starting with Cu(I) are shown in Fig. 1C, PVP3 (solid line), PVP4 (dotted line), BSA3 (dash line). The spectra show a slight amount of structure in the 300–500 nm region, which may be due to some direct bandgap transitions as previously seen by Klimov et al. in copper-deficient Cu_2S [30,31,64]. Also seen in a few of these samples is a small IR band similar to that observed in the green crystalline CuS. This might be due to some oxidation of Cu_2S into CuS. No room-temperature emission was detected for any of the samples, indicating that the relaxation pathways of the excited-state electrons follow primarily nonradiative pathways. This could be partly due to the indirect bandgap nature of Cu_xS.

ESR measurements

The ESR measurements of Cu^{2+} ions were performed at 110 K. Figures 2A and 2B show the results obtained on a few of the samples studied. Figure 2A shows the ESR spectra for the brown amorphous Cu_2S samples PVP1 (solid line) and BSA1 (dashed line). A shift of the Cu(II) ESR was observed for the BSA-containing sample, indicating Cu(II) binding with BSA. Figure 2B shows the ESR spectra for the green crystalline CuS samples PVP2 (solid line) and BSA2 (dashed line). It is interesting to notice that the brown samples display a Cu(II) signal, whereas the green samples do not. It is believed that the origin of the Cu(II) signal is from free Cu(II) ions in solution, rather than from Cu(II) ions in the nanoparticle lattice, as will be discussed later. Samples prepared starting with Cu(I) showed no Cu(II) ESR signal.

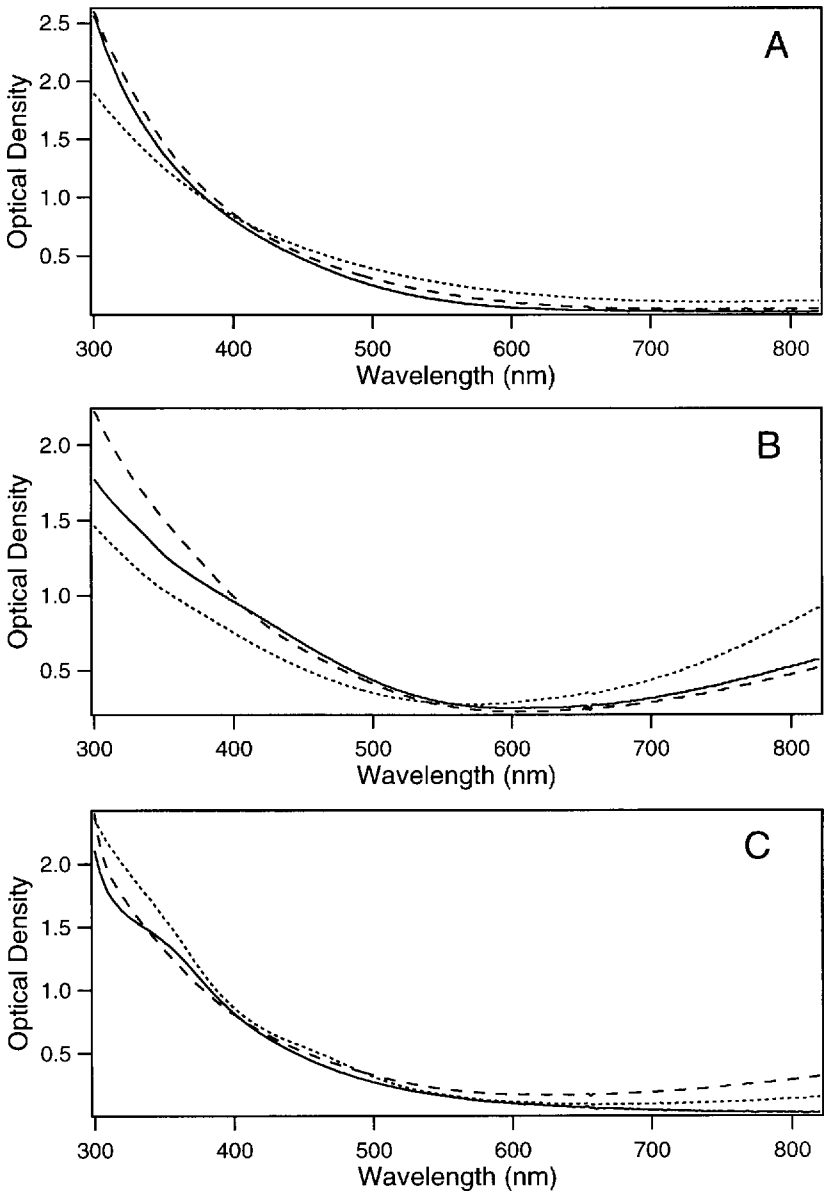

Fig. 1 Electronic absorption spectra of various Cu_xS nanoparticles. (A) Brown amorphous Cu_2S samples prepared with Cu(II) salts: PVP1 (solid), BSA1 (dashed), PEG1 (dotted). (B) Green crystalline CuS samples prepared with Cu(II) salts: PVP2 (solid), BSA2 (dashed), PEG2 (dotted). (C) Brown crystalline Cu_2S samples prepared with Cu(I) salts: PVP3 (solid), BSA3 (dashed), PVP4 (dotted).

Transient absorption/bleach measurements

Figure 3A shows the time evolution of the photoinduced electrons in aqueous brown amorphous Cu_2S (PEG1) colloids probed at 790 nm following excitation at 390 nm on long and short (inset) time scales. The transient absorption profiles feature a very fast rise followed by a double exponential decay with a

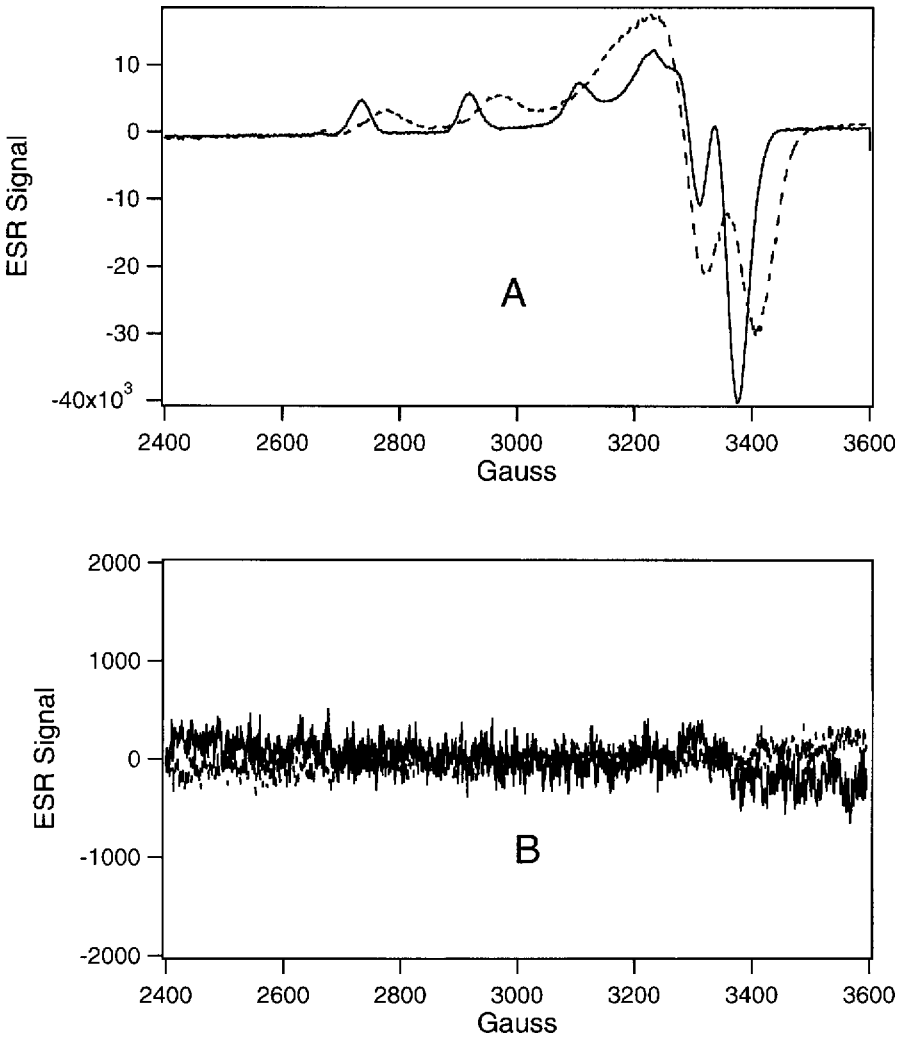

Fig. 2 Cu(II) ESR spectra of Cu_xS nanoparticles at ~110 K. (A).Brown amorphous Cu_2S samples prepared with Cu(II) salts: PVP1 (solid) and BSA1 (dashed) (B) Green crystalline CuS samples prepared with Cu(II) salts: PVP2 (solid) and BSA2 (dashed).

fast and slow component. The results fit well to a fast 1.1-ps exponential decay followed by a slower 80-ps decay. The fits are deconvolved with a Gaussian with full width at half-height (fwhm) of 200 fs to represent the instrument response.

The power dependence of the observed dynamics was investigated by varying the pump power from 1.5 μJ/pulse to 13 μJ/pulse. A few representative power-dependent results for sample PEG1 are shown in Fig. 3B. It was observed that the signal size was linearly proportional to pump power, indicating that the observed signals were from single photon excitation processes. All transient profiles could be fit with a double exponential decay with time constants of 1.1 ps and 80 ps. There is no power dependence of the time constants and of the relative amplitudes of the fast and slow decay components. This is similar to the power-independent electronic relaxation observed for Fe_2O_3 [39], AgI [38], PbI_2 [47], and Cu_2S [30,31,64] nanoparticles but in contrast to the strong power dependence of the electron

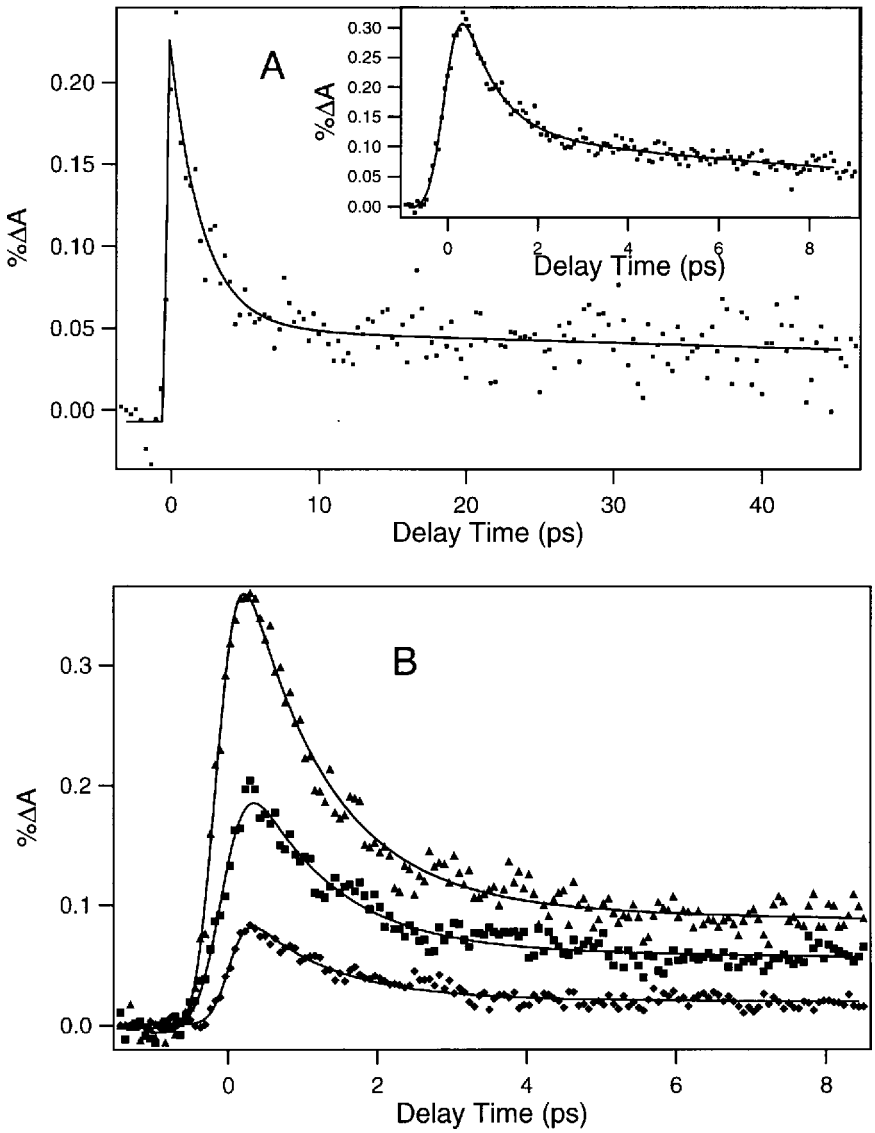

Fig. 3 (A). Transient absorption decay profiles of amorphous Cu_2S nanoparticles (PEG1) on long and short (inset) time scales. The data are fit using a nonlinear least-squares algorithm to a double exponential decay deconvolved with a Gaussian (200 fs fwhm) representing the instrument response. The data (dotted lines) are best fit with a double exponential with 1.1 ps and 80 ps times constants (solid lines). (B). Transient absorption decay profiles of amorphous Cu_2S nanoparticles (PEG1) acquired with 390-nm pump and 790-nm probe at different pump powers: 13.5 μJ/pulse (solid triangles), 6.8 μJ/pulse (solid squares), 3.4 μJ/pulse (solid diamonds). The solid lines are fits using the same fitting function and time constants as used in Fig.3A.

dynamics observed in other colloidal semiconductors such as CdS, CdSe [43], TiO_2 [71], $Cu_{1.96}S$, $Cu_{1.9}S$, and $Cu_{1.8}S$ [30,31,64]. The power-dependent dynamics have been attributed to exciton-exciton annihilation upon trap-state saturation for CdS, CdSe, and TiO_2 [43]. In the case of the copper-deficient sulfides, a nonlinear optical process observed was attributed to change in bandgap structure (indirect to direct) due to copper deficiency that led to a competition between direct and indirect bandgap relaxations.

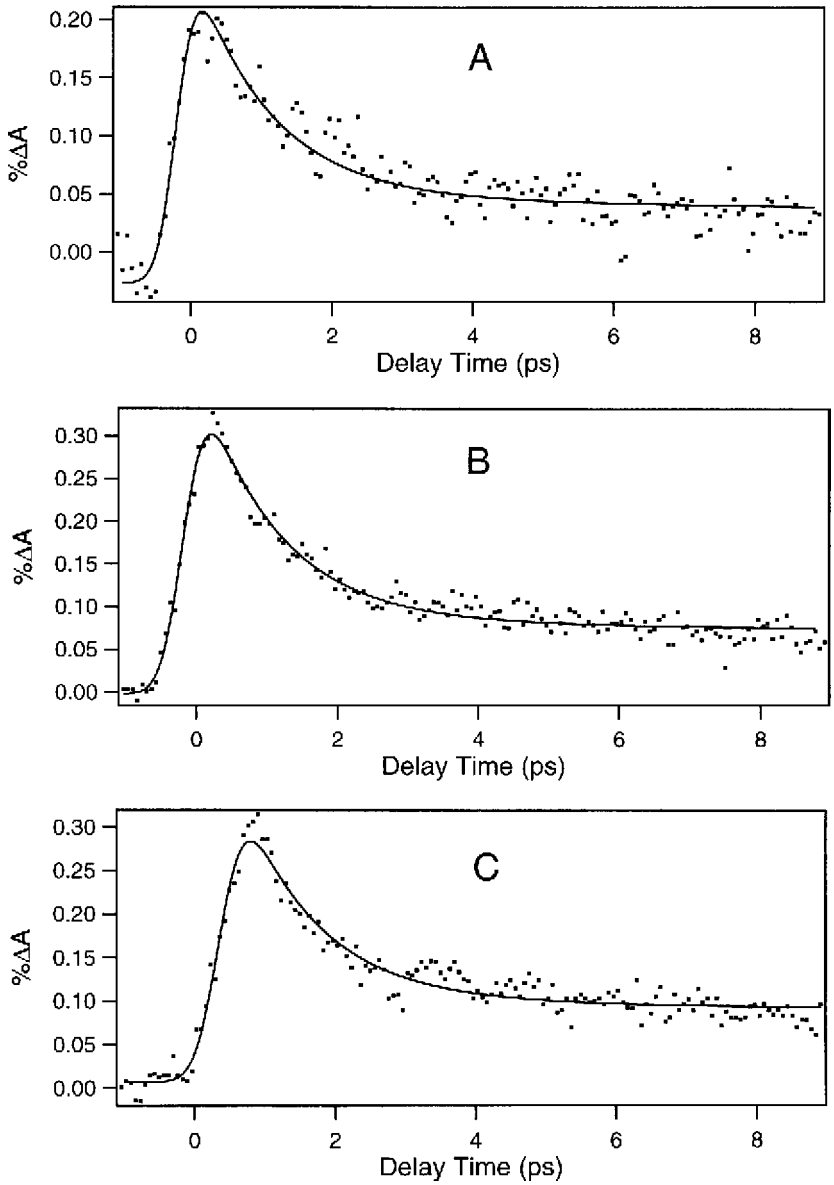

Fig. 4 Probe wavelength dependence on the transient absorption decay profiles of amorphous Cu_2S nanoparticles (PEG1) acquired with 390-nm pump and (A) 720-nm (B) 790-nm (C) 850-nm probe wavelengths. The solid lines are fits using the same fitting function and time constants as used in Fig.3A.

The probe wavelength dependence of the dynamics of amorphous Cu_2S (PEG1) was also investigated. Figure 4 shows the normalized dynamics observed at three different wavelengths: (A) 720 nm, (B) 790 nm, and (C) 850 nm. Within the S/N ratio, the dynamics are identical at these wavelengths and can be fit with the same function and time constants. This indicates that the transient absorption spectrum of the photoinduced electron is broad and fully developed within the laser pulse (~150 fs), similar to that observed in other semiconductor colloidal systems [25,38,39,72].

Figure 5 shows the normalized time evolution of the photoinduced electrons of two brown amorphous Cu_2S samples PVP1 (solid line) and BSA1 (dashed line), respectively, probed at 790 nm. The

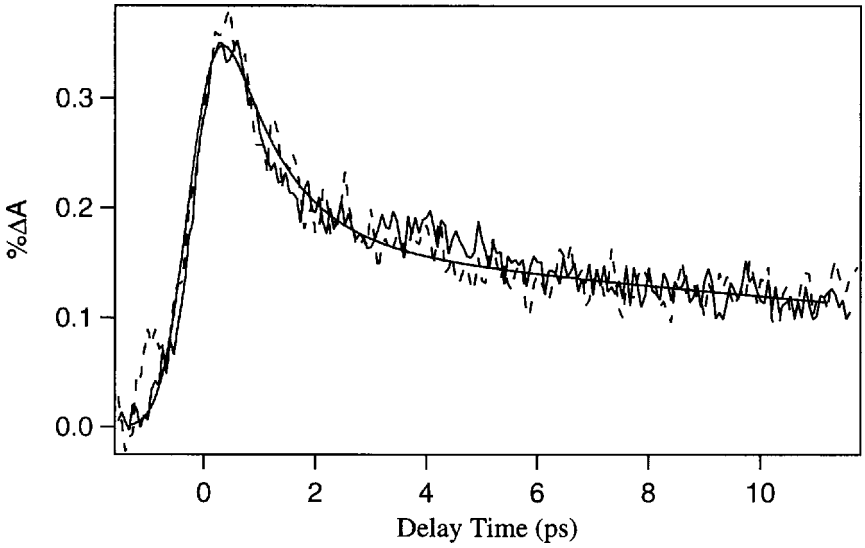

Fig. 5 Stabilizer dependence of the normalized transient absorption decay profiles acquired with 390-nm pump and 790-nm probe wavelength of PVP-stabilized amorphous Cu_2S nanoparticles (PVP1, solid line) and BSA-stabilized amorphous Cu_2S nanoparticles (BSA1, dash line).

smooth solid line is the double exponential fit using the same function and time constants as discussed above. Within S/N ratio, there was no observable difference in the dynamics between the two samples.

The electron dynamics of Cu_xS nanoparticles prepared in the green crystalline CuS form were studied as a function of excitation intensity. Figure 6 shows the normalized time evolution of the photo-

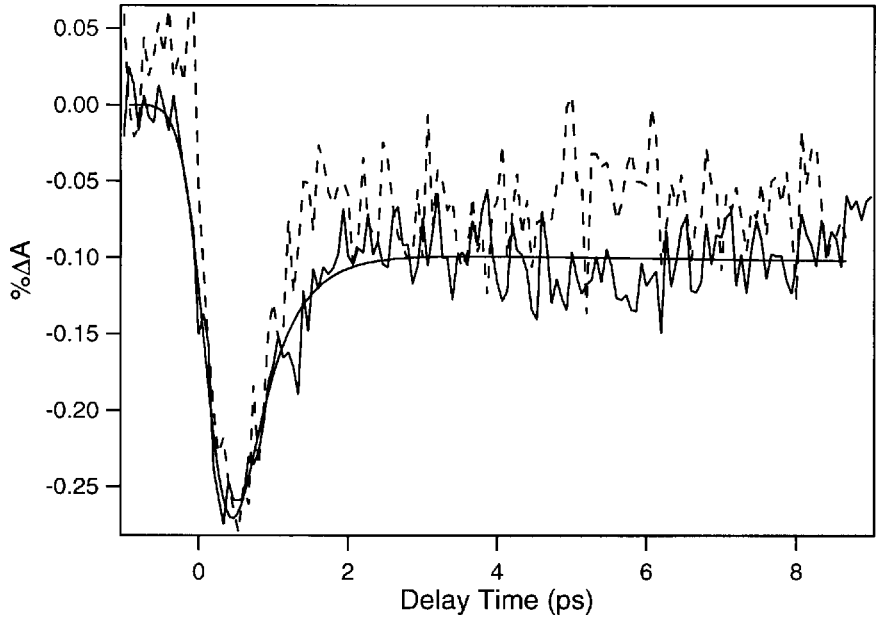

Fig. 6 Normalized transient bleach recovery profiles of crystalline CuS samples probed at 790 nm following photoexcitation at 390 nm at ~4 μJ/pulse: PVP2 (solid) and BSA2 (dashed). The smooth solid line is a fit using a deconvolved single exponential function with a time constant of 430 fs plus a long-lived offset.

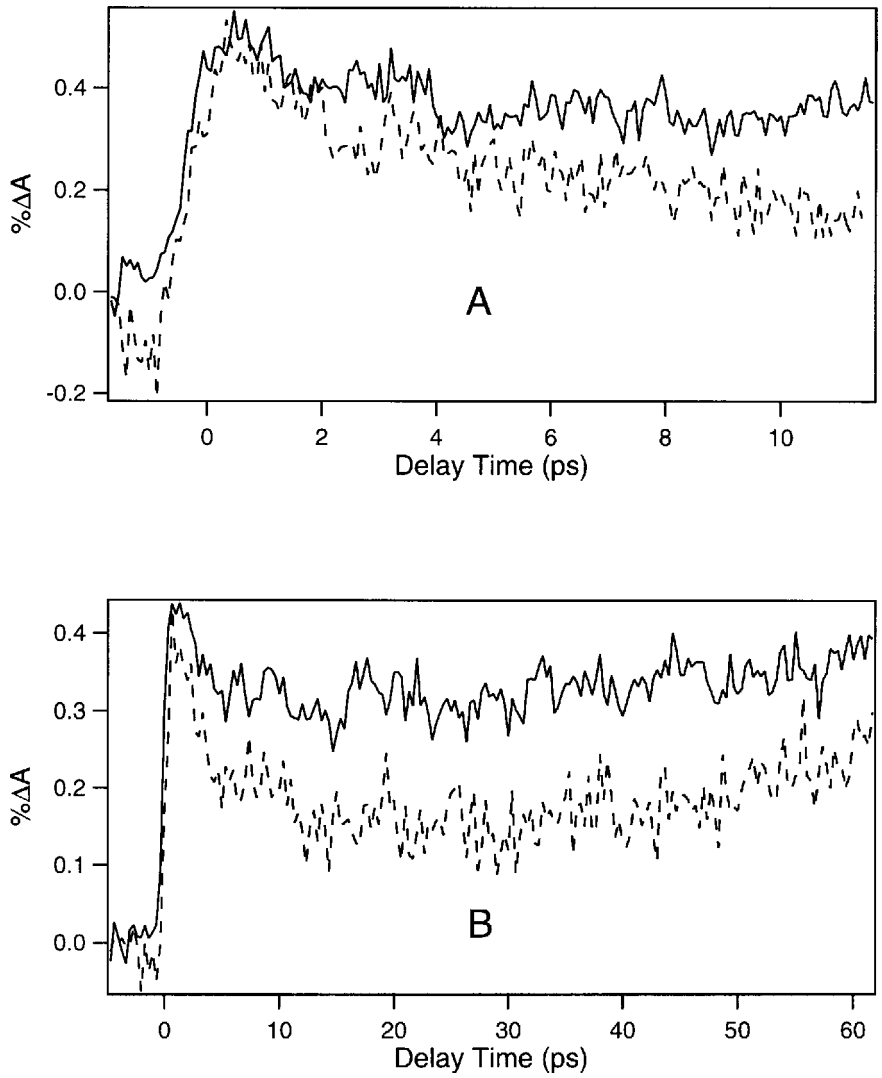

Fig. 7 Normalized transient absorption decay profiles of crystalline CuS samples probed at 790 nm following photoexcitation at 390 nm at ~12 μJ/pulse on (A) short and (B) long time scales: PVP2 (solid) and BSA2 (dashed).

induced electrons in two of the green samples, PVP2 (solid line) and BSA2 (dashed line) probed at 790 nm with excitation of ~4 μJ/pulse. Sample PEG2 showed identical results (data not shown). The observed dynamics are dramatically different from those of the brown samples. The dynamics feature a fast pulse-width limited bleach followed by a single exponential 430 fs recovery and a long-lived offset. The observed bleach is due to the depletion of population that absorbs the probe wavelength. Interestingly, at higher excitation intensities the green samples showed a transient absorption rather than a transient bleach signal, which is similar to that observed in Ag_2S nanoparticles [45]. For example, Fig. 7 shows similar measurements with excitation of 12 μJ/pulse. At this power, the two samples show dynamics similar at early times, a fast pulse-width limited rise followed by a fast 1.1 ps decay, but different on longer time scales. The longer time scales (Fig. 7B) showed a slow rise for both samples.

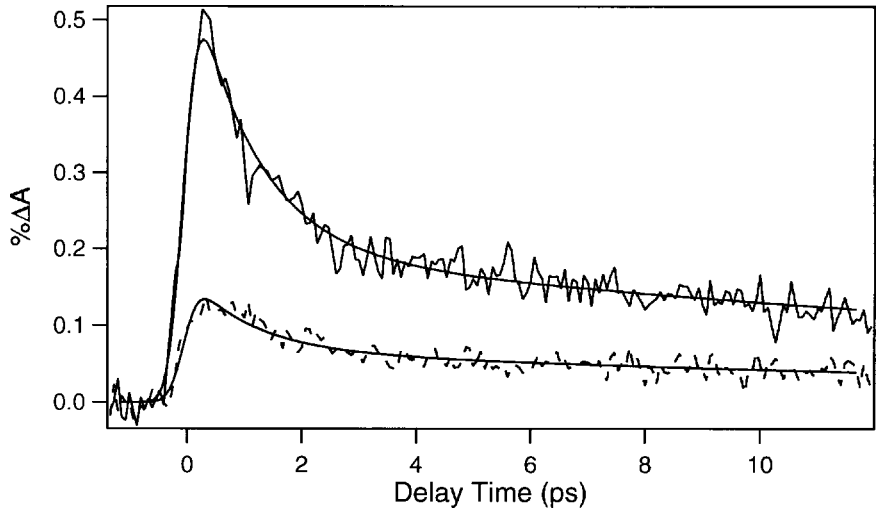

Fig. 8 Comparison of the transient absorption decay profiles of samples prepared with copper salts of Cu(II) (PVP1, solid line) or Cu(I) (PVP3, dashed line).

Figure 8 shows the time evolution of the photoinduced electrons in Cu_xS samples prepared with either Cu^{2+} (PVP1, solid line) or Cu^{+} (PVP3, dashed line). This was done to compare the dynamics of brown crystalline Cu_2S and brown amorphous Cu_2S. Femtosecond studies have been performed on crystalline Cu_2S in a glass matrix by Klimov et al. [30,31,64] but have not been performed in liquids. The dynamics for the two samples can be fit with the same function and time constants as described, but rather different signal sizes, which may be due to the difference in crystal structure of the nanoparticles.

DISCUSSION

Nature of the IR band and the associated middle-gap state

The nature of the IR band is a central issue in discussing the difference between the different types of Cu_xS samples. Many studies have been conducted to elucidate the nature of the IR band and the associated state within the bandgap [60,63,65,66,68–70]. As can be seen in Figs. 1A and 1B, the IR band appeared when the brown amorphous Cu_2S (Fig. 1A), which was stable for weeks at 4 °C, turned into the green crystalline CuS (Fig. 1B) when exposed to air and heating. The green samples remained stable for months at room temperature. This seems to support the suggestion that brown amorphous Cu_2S is a metastable form which may convert to the thermodynamically more stable form of crystalline CuS [66,70]. Thus, the presence of Cu(II) correlates with the appearance of the IR band.

In the picosecond studies by Artemyev et al. [65,68,69], brown Cu_xS samples were converted to green by heating, resulting in the appearance of the IR absorption band. The IR band was attributed to a state in the bandgap due to surface oxidation, which lies 1 eV below the conduction band. It was believed that this new middle-gap state was occupied by electrons and thus has electron-donor character. The IR band is assigned to the transition from this middle-gap state to the conduction band, based on the following observations. When excited at 540 nm or 1080 nm, similar transient absorption dynamics were observed in the green CuS sample. This is taken as an indication that the same final state, presumably the conduction band or trap state, was reached with 540-nm or 1080-nm excitation. It was proposed that the 1080-nm excitation initiated from an occupied state above the top of the valence band

and was responsible for the IR absorption in the ground state. Since the 540-nm absorption is mainly due to a transition from the valence band to the conduction band, it should start from a different initial state compared to the 1080-nm absorption. However, transient bleach data showed that the ground-state recovery dynamics were similar following excitation at 540 nm or 1080 nm, which would seem to suggest that the two initial states were the same. To reconcile the apparent contradiction, the authors claimed that the 540-nm absorption contains contribution from a transition starting from the middle-gap state to the conduction band.

There appears to be some inconsistencies with the above model. The most obvious one is the problem with the similar dynamics for the final state (based on transient absorption) and for the initial state (based on transient bleach). If both 540-nm and 1080-nm excitations initiated from the middle-gap state, the final states should be very different, and the transient absorption dynamics are thus expected to change. If the two excitations initiated from two different states and ended in the same final state, the final-state dynamics based on transient absorption should be similar, but the ground-state recovery based on bleach should be different. Second, the middle-gap state was suggested to have electron-donor character, i.e. occupied, based on the claim that an induced transient absorption from a 1080-nm excitation into the middle-gap state from the valance band is unreasonable. This claim, however, is in direct contradiction to their claim that an electron in the middle-gap state can be excited into the conduction band by the 1080-nm excitation. If an electron can be excited from this middle-gap state, then it should just as easily be probed from this middle-gap state to give induced transient absorption. Finally, from their suggestion that both the IR and UV-blue absorptions are due to transitions from the middle-gap state to the conduction band, one would expect that there should be continuous absorption between the IR and the UV, which is in contrast to experimental observation.

An alternative explanation for the middle-gap state is that it is an electron-acceptor state or unoccupied. The IR absorption band would then correspond to a transition from the valance band to this state. This proposal is consistent with data obtained from electronic absorption, ESR, and transient absorption/bleach dynamics. First, when the IR band appeared during the conversion from the brown to the green sample, there is little change in the UV-blue region of the spectrum, indicating little change in the states responsible for the UV-blue absorption. This can be understood if one supposes that the middle-gap state is unoccupied and the IR absorption is due to transition from the valence band to this unoccupied state. In that case, the absorption in the UV-blue region is not expected to change significantly. Second, since transient bleach was observed within the laser-pulse for the green CuS when excited at 390 nm and probed at 790 nm, the 790-nm and 390-nm transitions must be from the same initial state, presumably the valence band, rather than from two different initial states [65,68,69]. Third, ESR measurements of our samples seemed to suggest that the green CuS samples contain Cu(II) ions that should behave as electron acceptors. As mentioned earlier, Cu(II) signal was observed in all amorphous brown samples, and no signal was observed for the green or crystalline brown samples. Since the Cu ions inside the nanoparticles of the amorphous brown samples are believed to be in the Cu(I) oxidation state, they should not give any ESR signal. Therefore, the observed Cu(II) signal is attributed to free Cu(II) ions in solution, most likely due to incomplete reaction with Na_2S or H_2S. This is supported by the observation of a shift of the ESR spectrum for BSA containing samples (Fig. 2A, dashed line) due to BSA-Cu(II) binding complex as well as an observed shift due to pH indicating the Cu(II) was free in solution. Upon thermal conversion to green crystalline CuS, it is possible that the free Cu(II) ions oxidize some of the Cu(I) in the nanoparticles to Cu(II) or that the free Cu(II) ions may replace the Cu(I) ions in the nanoparticle lattice, thereby reducing or eliminating the Cu(II) ESR signal. The Cu(II) ions inside the nanoparticles are not expected to give an ESR signal because they are strongly coupled due to ionic bonding through sulfur anions [73,74]. These data support the claim that the amorphous brown Cu_xS is a metastable Cu_2S state comprised of Cu(I), whereas the green Cu_xS is a true crystalline covellite, CuS, with Cu(II) incoporated in the lattice. These Cu(II) ions may be responsible for the IR band and the associated middle-gap state that should have electron-acceptor characters.

Charge-carrier dynamics

Before elaborating on the assignment of the observed dynamics, a few possibilities should be discussed about the origin of the transient absorption signal, including free charge carriers (hot or thermalized), excitons, and trapped charge carriers. In previous studies of other semiconductor nanoparticles, it was found that transient absorption in the red to near infrared region is dominated by deep-trapped carriers on long time scales and at low excitation intensities [30,38,43,45,75]. On short (a few to a few tens of picoseconds) time scales, free carriers, excitons, or shallow-trapped carriers can have significant contributions [30,38,43–45,71,76]. The transient absorption signal at early times is attributed to charge carriers at the bottom of the conduction band, excitons, or shallow traps, and at longer times becomes dominated by deep-trapped charge carriers.

Based on the above assignment of transient absorption signals and previous work [30,31,64,65,68,69], we propose to interpret the observed dynamics of the brown Cu_2S as follows. Immediately following photoexcitation, the initially formed hot electrons thermalize quickly, within the excitation pulse of ~150 fs, to the bottom of the conduction band (CB) or the excitonic state. The electrons at the conduction band edge are partly responsible for the transient absorption signal at short times. The observed 1.1-ps decay is attributed to relaxation from the band edge to shallow traps (ST). Direct recombination on this time scale should be insignificant due to the indirect bandgap nature of Cu_2S. The electrons can further relax from the shallow trap states into deep traps (DT), to which we attribute the 80-ps decay component. This is consistent with the results from Artemeyev et al. that showed a very fast shallow trapping (unresolved) followed by deep trapping on a time scale of 80–100 ps [65,68,69].

Compared to the brown Cu_2S samples, the green crystalline CuS samples showed very different dynamics due to the presence of the IR absorption band and the middle-gap state. Upon photoexcitation at 390 nm, the ground state was depleted and gave rise to the observed bleach signal at the probe wavelength (790 nm). At the same time, electrons promoted into the conduction band and trap states could absorb the probe light to give rise to induced absorption. As a result, the signal observed has contributions from bleaching of the ground state and transient absorption of conduction band and trapped charge carriers. At low excitation energies, the bleach is the dominant signal, indicating that the absorption cross-section of the ground state is greater than that of the excited state. Following a pulse-width limited bleach, the signal recovered with a 430-fs time constant plus an offset. The fast 430-fs recovery is assigned primarily to trapping, with the offset assigned to deep trapping and recombination. At higher pump excitation intensities, the bleach is no longer observed, and transient absorption becomes dominant, similar to that observed in Ag_2S nanoparticles [45]. This can be explained via trap-state saturation as has been proposed for CdS [43] and Ag_2S [45]. At high excitation intensities, a build-up of electrons may occur in the conduction band due to trap-state saturation. The recovery of the ground state may become slower since trap-state saturation will effectively block some of the relaxation pathways that are otherwise mediated by the trap states. The population build-up in the conduction band can lead to more dominant transient absorption over bleach. This power dependence and trap-state saturation suggests the possibility that crystalline CuS may be used as a saturable absorber for lasers operating at wavelengths longer than ~700 nm, as has been suggested previously [65,68,69].

Modeling of relaxation dynamics

To gain further insight into the energy relaxation mechanism in the Cu_xS nanoparticles, we have used a simple four-state kinetic scheme to model the observed dynamics, as shown in Fig. 9. The scheme includes the valence band (VB), the conduction band (CB), shallow traps (ST), and deep traps (DT). With the proper combination of rate constants, the scheme leads to a double exponential decay of the CB, a fast exponential rise followed by a slow exponential decay of the ST, a slow rise of the DT, and

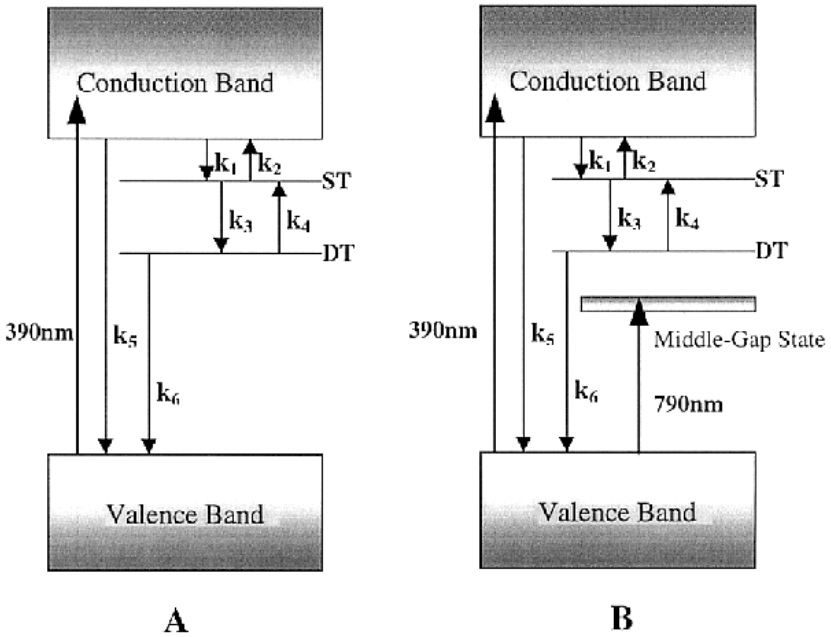

Fig. 9 Proposed energy level diagram for (A) Cu_2S and (B) CuS used in kinetic modeling of the transient absorption/bleach data. The middle-gap state might be more appropriately labeled as a middle-gap band.

double exponential recovery of the VB. By combining different contributions from the different states with a specific set of rate constants, we are able to closely fit our observed data. The rate constants were chosen based on these and previous experiments discussed [30,31,64,65,68,69]. Contributions from the individual states to the signal were chosen as approximations and modified from iterative applications of the model to fit the experimental data. Using the following sets of rate constants: $k_1 = 1.5\ ps^{-1}$, $k_2 = 2.0 \times 10^{-1}\ ps^{-1}$, $k_3 = 1.3 \times 10^{-2}\ ps^{-1}$, $k_4 = 1.0 \times 10^{-3}\ ps^{-1}$, $k_5 = 2.0 \times 10^{-3}\ ps^{-1}$, and $k_6 = 2.0 \times 10^{-3}\ ps^{-1}$, and with 80% contribution from CB, 15% from ST, and 5% from DT, we were able to generate curves which closely fit the dynamics data of both amorphous and crystalline Cu_2S. In this case, there is no contribution from the VB since there is no bleach possible at the probe wavelength.

In modeling the data for crystalline CuS, the VB needs to be included explicitly since it is probed by the probe pulse and reflected as a transient bleach signal (Fig. 9B). Rate constants and state contributions were chosen similarly as for Cu_2S. The rate constants used for Cu_2S work equally well for crystalline CuS except k_1 was increased to $2.0\ ps^{-1}$. By combining 40% contribution from VB, 15% from CB, 22.5%, from ST, and 22.5% from DT, a curve could be generated which fit the observed low-excitation intensity data. In modeling the dynamics at high powers, we found that it is primarily the saturation of the shallow trap states that results in accumulation of electrons in the conduction band and thus increased transient absorption over bleach. This is probably because relaxation from CB to ST is much faster than from ST to DT, and high-intensity excitation leads to accumulation of electrons in ST states, and thereby saturation, more easily than in DT states. In this modeling, the middle-gap state was not explicitly included. Its effect on the dynamics is probably similar to that of deep trap states.

SUMMARY

In summary, we have performed the first direct femtosecond measurements of the dynamics of photoinduced electrons in crystalline CuS and amorphous and crystalline Cu_2S nanoparticles in solution.

In both types of Cu_2S samples, a dominant fast decay component and a slower decay component were observed and found to be independent of excitation intensity, probe wavelength, and capping agent. The fast decay (1.1 ps) is attributed to charge-carrier trapping at shallow trap sites, while the long decay (80 ps) component is assigned primarily to deep trapping and recombination. The dynamics of crystalline CuS showed interesting power dependence. At low excitation intensities, a bleach was observed with a fast recovery (430 fs) followed by a long time offset. The fast recovery is primarily due to electron trapping to shallow traps and the long time offset is assigned to electronic relaxation from shallow to deep traps and further relaxation from deep traps. At high excitation intensities, a transient absorption signal with a 1.1 ps decay and a slow rise was seen. The power dependence of the crystalline CuS was attributed to trap-state saturation at high intensities. From the kinetic modeling, the electronic relaxation dynamics for both types of Cu_2S and CuS nanoparticles are found to be dominated by trap states, most likely due to a high density of surface states. Based on the dynamics data, ESR measurements, and electronic absorption spectra, we suggest that the IR band in the green CuS samples is due to transition from the valence band to the middle-gap state with electron-acceptor characters.

ACKNOWLEDGMENTS

M.C.B. and J.Z.Z. acknowledge financial support from the Petroleum Research Fund administered by the American Chemical Society, Collaborative UC Los Alamos Research Fund (CULAR), and the Faculty Research Fund of UC Santa Cruz. R.K.M. and C.L.T. acknowledge the financial support of a CULAR grant and from UCR Academic Senate.

REFERENCES

1. L. E. Brus. *J. Phys. Chem.* **79**, 5566–5571 (1983).
2. L. E. Brus. *IEEE J. Quant. Elec.* **22**, 1909–1914 (1986).
3. J. H. Fendler. *Chem. Rev.* **87**, 877–899 (1987).
4. M. Gratzel. *Heterogeneous Photochemical Electron Transfer*, CRC Press, Boca Raton (1989).
5. A. Henglein. *Chem. Rev.* **89**, 1861–1873 (1989).
6. M. L. Steigerwald and L. E. Brus. *Acc. Chem. Res.* **23**, 183–188 (1990).
7. Y. Wang. *Acc. Chem. Res.* **24**, 133–139 (1991).
8. P. V. Kamat. *Prog. Reac. Kin.* **19**, 277–316 (1994).
9. J. R. Heath. *Science* **270**, 1315–1316 (1995).
10. C. B. Murray, C. R. Kagan, M. G. Bawendi. *Science* **270**, 1335–1338 (1995).
11. A. P. Alivisatos. *J. Phys. Chem.* **100**, 13226–13239 (1996).
12. J. R. Heath, R. S. Williams, J. J. Shiang, S. J. Wind, J. Chu, C. Demic, W. Chen, C. L. Stanis, J. J. Bucchignano. *J. Phys. Chem.* **100**, 3144–3149 (1996).
13. M. Nirmal, B. O. Dabbousi, M. G. Bawendi, J. J. Macklin, J. K. Trautman, T. D. Harris, L. E. Brus. *Nature* **383**, 802–804 (1996).
14. P. V. Kamat. *Prog. Inorg. Chem.* **44**, 273–343 (1997).
15. J. Z. Zhang. *Acc. Chem. Res.* **30**, 423–429 (1997).
16. P. Roussignol, M. Kull, D. Ricard, F. de Rougemont, R. Frey, C. Flytzanis. *App. Phys. Lett.* **51**, 1882–1884 (1987).
17. N. Peyghambarian, B. Fluegel, D. Hulin, A. Migus, M. Joffre, A. Antonetti, S. W. Koch, M. Lindberg. *IEEE J. Quant. Elec.* **25**, 2516–2522 (1989).
18. M. G. Bawendi, W. L. Wilson, L. Rothberg, P. J. Carroll, T. M. Jedju, M. L. Steigerwald, L. E. Brus. *Phys. Rev. Lett.* **65**, 1623–1626 (1990).

19. N. P. Ernsting, M. Kaschke, H. Weller, L. Katsikas. *J. Opt. Soc. Am. B* **7**, 1630–1637 (1990).
20. M. Kaschke, N. P. Ernsting, U. Muller, H. Weller. *Chem. Phys. Lett.* **168**, 543–550 (1990).
21. J. L. Machol, F. W. Wise, R. C. Patel, D. B. Tanner. *Phys. Rev. B* **48**, 2819–2822 (1993).
22. R. W. Schoenlein, D. M. Mittleman, J. J. Shiang, A. P. Alivisatos, C. V. Shank. *Phys. Rev. Lett.* **70**, 1014–1017 (1993).
23. A. Eychmuller, T. Vossmeyer, A. Mews, H. Weller. *J. Lumin.* **58**, 223–226 (1994).
24. D. M. Mittleman, R. W. Schoenlein, J. J. Shiang, V. L. Colvin, A. P. Alivisatos, C. V. Shank. *Phys. Rev. B* **49**, 14435–14447 (1994).
25. J. Z. Zhang, R. H. O'Neil, T. W. Roberti. *J. Phys. Chem.* **98**, 3859–3864 (1994).
26. J. Z. Zhang, R. H. O'Neil, T. W. Roberti, J. L. McGowen, J. E. Evans. *Chem. Phys. Lett.* **218**, 479–484 (1994).
27. D. P. Colombo, K. A. Roussel, J. Saeh, D. E. Skinner, J. J. Cavaleri, R. M. Bowman. *Chem. Phys. Lett.* **232**, 207–214 (1995).
28. D. E. Skinner, D. P. Colombo, J. J. Cavaleri, R. M. Bowman. *J. Phys. Chem.* **99**, 7853–7856 (1995).
29. V. F. Kamalov, R. Little, S. L. Logunov, M. A. El-Sayed. *J. Phys. Chem.* **100**, 6381–6384 (1996).
30. V. I. Klimov, P. Haring-Bolivar, H. Kurz, V. A. Karavanskii. *Superlattices and Microstructures* **20**, 395–404 (1996).
31. V. I. Klimov and V. A. Karavanskii. *Phys. Rev. B.* **54**, 8087–8094 (1996).
32. N. J. Cherepy, G. P. Smestad, M. Gratzel, J. Z. Zhang. *J. Phys. Chem. B* **101**, 9342–9351 (1997).
33. R. Kennedy, I. Martini, G. Hartland, P. V. Kamat. *Proc. Ind. Acad. Sci.-Chem. Sci.* **109**, 497–507 (1997).
34. S. L. Logunov, T. S. Ahmadi, M. A. El-Sayed, J. T. Khoury, R. L. Whetten. *J. Phys. Chem. B* **101**, 3713–3719 (1997).
35. I. Martini, G. V. Hartland, P. V. Kamat. *J. Phys. Chem. B* **101**, 4826–4830 (1997).
36. I. Martini, J. Hodak, G. V. Hartland, P. V. Kamat. *J. Chem. Phys.* **107**, 8064–8072 (1997).
37. B. A. Smith, D. A. Waters, A. E. Faulhaber, M. Kreger, J. Z. Zhang. *J. Sol-Gel Sci. Tech.* **9**, 125–137 (1997).
38. M. C. Brelle and J. Z. Zhang. *J. Chem. Phys.* **108**, 3119–3126 (1998).
39. N. J. Cherepy, D. B. Liston, J. A. Lovejoy, H. M. Deng, J. Z. Zhang. *J. Phys. Chem. B* **102**, 770–776 (1998).
40. H. N. Ghosh, J. B. Asbury, Y. X. Weng, T. Q. Lian. *J. Phys. Chem. B* **102**, 10208–10215 (1998).
41. S. Logunov, T. Green, S. Marguet, M. A. El-Sayed. *J. Phys. Chem. A* **102**, 5652–5658 (1998).
42. I. Martini, J. H. Hodak, G. V. Hartland. *J. Phys. Chem. B* **102**, 607–614 (1998).
43. T. W. Roberti, N. J. Cherepy, J. Z. Zhang. *J. Chem. Phys.* **108**, 2143–2151 (1998).
44. J. B. Asbury, R. J. Ellingson, H. N. Ghosh, S. Ferrere, A. J. Nozik, T. Q. Lian. *J. Phys. Chem. B* **103**, 3110–3119 (1999).
45. M. C. Brelle, J. Z. Zhang, L. Nguyen, R. K. Mehra. *J. Phys. Chem. A* in press (1999).
46. C. Burda, T. C. Green, S. Link, M. A. El-Sayed. *J. Phys. Chem. B* **103**, 1783–1788 (1999).
47. A. Sengupta, B. Jiang, K. C. Mandal, J. Z. Zhang. *J. Phys. Chem. B* **103**, 3128–3137 (1999).
48. C. T. Dameron, R. N. Reese, R. K. Mehra, A. R. Kortan, P. J. Carroll, M. L. Steigerwald, L. E. Brus, D. R. Winge. *Nature* **338**, 596–597 (1989).
49. C. T. Dameron and D. R. Winge. *Inorg. Chem.* **29**, 1343–1348 (1990).
50. A. L. Rogach, L. Katsikas, A. Kornowski, D. S. Su, A. Eychmuller, H. Weller. *Ber. Bun. Ges.* **100**, 1772–1778 (1996).

51. W. O. Bae, R. Abdullah, D. Henderson, R. K. Mehra. *Biochem. Biophys. Res. Comm.* **237**, 16–23 (1997).
52. W. Bae, R. Abdullah, R. K. Mehra. *Chemosphere* **37**, 363–385 (1998).
53. W. Bae and R. K. Mehra. *J. Inorg. Biochem.* **70**, 125–135 (1998).
54. W. Bae and R. K. Mehra. *J. Inorg. Biochem.* **69**, 33–43 (1998).
55. L. Nguyen, R. Kho, W. Bae, R. J. K. Mehra. *Chemosphere* **38**, 155–173 (1999).
56. C. L. Torres-Martinez, L. Nguyen, R. Kho, W. Bae, K. Bozhilov, V. Klimov, R. K. Mehra. *Nanotechnology* **10**, 340–354 (1999).
57. O. H. Lowry, N. R. Rosebrough, A. L. Farr, R. J. Randall. *J. Biol. Chem.* **193**, 265–275 (1951).
58. D. L. Perry and J. A. Taylor. *J. Mat. Sci. Lett.* **5**, 384–386 (1986).
59. H. Nozaki, K. Shibata, N. Ohhashi. *J. Sol. St. Chem.* **91**, 306–311 (1991).
60. E. J. Silvester, F. Grieser, B. A. Sexton, T. W. Healy. *Langmuir* 7, 2917–2922 (1991).
61. H. J. Gotsis, A. C. Barnes, P. Strange. *J. Phys.* **4**, 10461–10468 (1992).
62. C. Sugiura, H. Yamasaki, T. Shoji. *J. Phys. Soc. Jap.* **63**, 1172–1178 (1994).
63. I. Grozdanov, M. Najdoski. *J. Sol. St. Chem.* **114**, 469–475 (1995).
64. V. Klimov, P. Haring Bolivar, H. Kurz, V. Karavanskii, V. Krasovskii, Y. Korkishko. *App. Phys. Lett.* **67**, 653–655 (1995).
65. M. V. Artemyev, V. S. Gurin, K. V. Yumashev, P. V. Prokoshin, A. M. Maljarevich. *J. App. Phys.* **80**, 7028–7035 (1996).
66. H. Grijalva, M. Inoue, S. Boggavarapu, P. Calvert. *J. Mat. Chem.* **6**, 1157–1160 (1996).
67. S. H. Saito, H. Kishi, K. Nie, H. Nakamaru, F. Wagatsuma, T. Shinohara. *Phys. Rev. B* **55**, 14527–14535 (1997).
68. K. V. Yumashev, A. M. Malyarevich, P. V. Prokoshin, M. V. Artem'ev, V. S. Gurin, V. P. Mikhailov. *Kvan. Elek. Mos.* **24**, 741–745 (1997).
69. K. V. Yumashev, P. V. Prokoshin, A. M. Malyarevich, V. P. Mikhailov, M. V. Artemyev, V. S. Gurin. *App. Phys. B* **B64**, 73–78 (1997).
70. K. M. Drummond, F. Grieser, T. W. Healy, E. J. Silvester, M. Giersig. *Langmuir* in press (1999).
71. R. M. Bowman, D. E. Skinner, J. Colombo, D.P., J. J. Cavaleri. *J. Phys. Chem.* **99**, 7853–7856 (1995).
72. G. Rothenberger, J. Moser, M. Grätzel, N. Serpone, D. K. Sharma. *J. Am. Chem. Soc.* **107**, 8054–8059 (1985).
73. A. Abragam and B. Bleaney. *Electron Paramagnetic Resonance of Transition Ions*, Claredon Press, Oxford (1970).
74. F. E. Mabbs, D. Collision. *Electron Paramagnetic Resonance of d Transition Metal Compounds*, Elsevier, London (1992).
75. M. O'Neil, J. Marohn, G. McLendon. *Chem. Phys. Lett.* **168**, 208–210 (1990).
76. R. R. Alfano, K. Shum, W. B. Wang, K. M. Jones. *Phys. Rev. Lett.* **68**, 3904–3907 (1992).